Photovoltaic application of architecture ITO/graphene oxide–polyaniline/aluminum

M. S. Katore, K. R. Nemade, S. S. Yawale & S. P. Yawale

Journal of Materials Science: Materials in Electronics

ISSN 0957-4522

J Mater Sci: Mater Electron
DOI 10.1007/s10854-016-5049-5

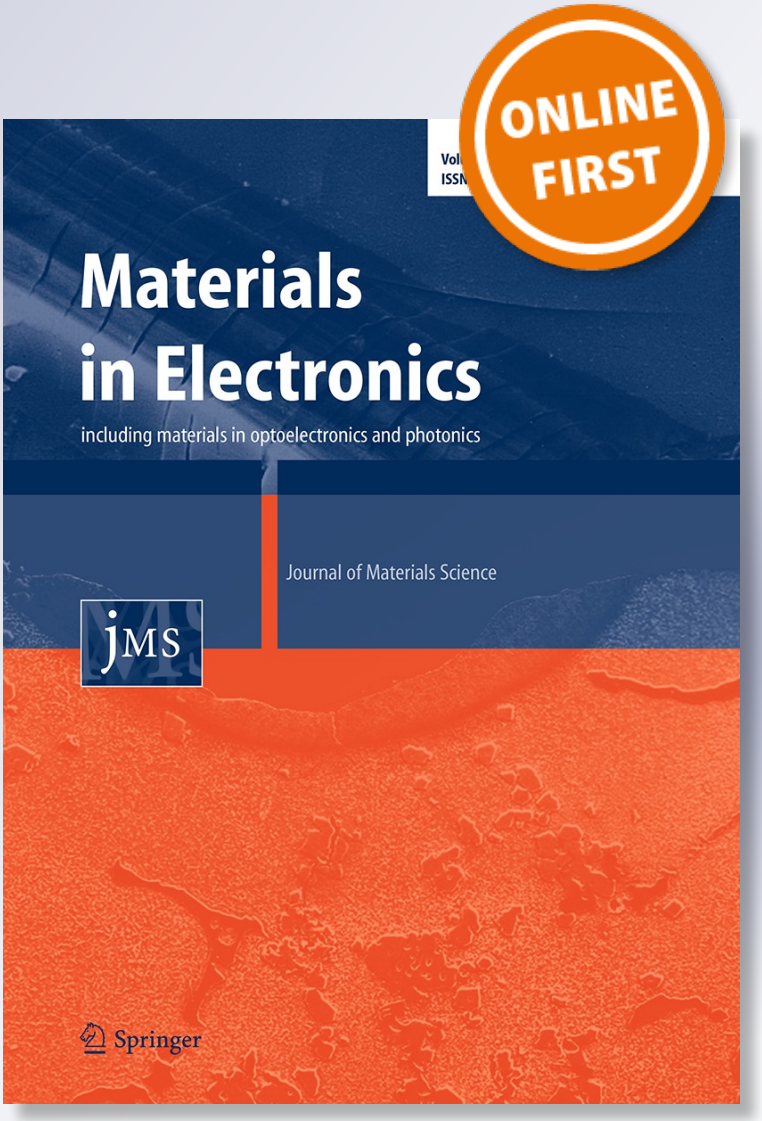

Springer

J Mater Sci: Mater Electron
DOI 10.1007/s10854-016-5049-5

Photovoltaic application of architecture ITO/graphene oxide–polyaniline/aluminum

M. S. Katore[1] · K. R. Nemade[2] · S. S. Yawale[1] · S. P. Yawale[1]

Received: 6 November 2015 / Accepted: 22 May 2016

Abstract Through present article, we reported chemically engineered graphene oxide (GO) loaded polyaniline (PANi) matrix of architecture ITO/graphene oxide–polyaniline/aluminum for photovoltaic application. The photovoltaic behaviors of GO loaded PANi matrix analyzed as a function of concentration of GO. The photovoltaic response of prepared photovoltaic cell shows good dependence on concentration of GO in PANi matrix. The increase in power conversation efficiency attributed to good optical properties of GO in visible region. The as-fabricated PV cells generated stable photocurrent and photovoltage under light illumination.

1 Introduction

The increasing cost of energy has been serious problem for developing countries. In order to fulfill this demand of energy, generally conventional sources of energies are used. But, conventional ways of production of energy results in pollution of environment. The effective solution for this problem is to use clean source of energy that is solar energy. Thus, the development of efficient solar cell technology is one of the main challenges for the researchers and engineers working in this area. Now a day, photovoltaic cells technology is mainly dominated by silicon based cell. Organic solar cells also have good market due to their photovoltaic conversion efficiency and good performance. The conducting polymer plays a crucial role in the device fabrication of photovoltaic cell. Conducting polymer such as polypyrrole, polyaniline, polythiophene etc. exhibits good photovoltaic characteristics. In order to resolve the some problems associates with conducting polymer based PV cell technology, metal oxide doped conducting polymer are used, which is importance class of materials science for photovoltaic application.

Recently, Ebrahim et al. [1] reported the dye-sensitized solar cell based on PANi/multiwalled carbon nanotubes composite as a counter electrode. The electrical properties of fabricated devices analyzed using by measuring current density, voltage, capacitance voltage, and impedance under both dark and illuminated conditions. In this study, energy conversion efficiency of photovoltaic cell was 0.224 %. Mozaffari et al. [2] studied the solar cell application of nano Pt/G/polyaniline, under illumination with a simulated solar light of 100 mW cm^{-2}, in which power conversion efficiency was found to be 6.19 %, which is 29 % higher than that of the cell with PANi counter electrode. The dye sensitized solar cell based on PANi base indium–tin oxide shows the energy conversion efficiency (η) of the order of 0.462 % [3]. Abdulrazzaq et al. [4] studied the effect of degree of protonation in PANi on efficiency of solar cells. In different three protonation concentrations of PANi are zero-protonated, half-protonated, and fully protonated thin films, current–voltage measurements shows that conversion efficiency of 1.3 %. Huang et al. [5] prepared hollow spherical PANi particles on an ITO/glass substrate to prepare a counter electrode for a dye-sensitized solar cell. The results show that the film consisting of PANi particles has a potential for the replacement of Pt in dye-sensitized solar cell. Mangal et al. [6] studied the photovoltaic response of aluminum/polyaniline/GaAs metal–insulator–semiconductor

✉ M. S. Katore
mayurkatore2015@gmail.com

[1] Department of Electronics, Government Vidarbha Institute of Science and Humanities, Amravati 444 604, India

[2] Department of Physics, Indira Mahavidyalaya, Kalamb 445 401, India

Published online: 03 June 2016

diode. The highest of efficiency was found to be 5.2 %. In this study, thickness of PANi plays an important role for determining various parameters of diode. The tunneling mechanism was employed to understand the findings of this paper. Huang synthesized Zn/TiO_2 materials by employing agarose gel as a template. The results shows that undoped sample exhibits efficiency of the order of 6.7 % and 0.5 at.% sample showed efficiency value 7.6 %. It is observed that further doping decreases the performance of the device [7]. Wu et al. [8] have reported the enhancement in efficiency of solar cell by using transparent PANi electrode. The thin films of PANi on transparent indium–tin-oxide electrodes by electrodeposition of aniline in an aqueous H_2SO_4 electrolyte solution, fabricated solar cells generated stable photocurrent and photovoltage under light illumination [9]. Solar cell with architecture Muscovite/TiO_2/Dye/Al shows maximum efficiency of the order of 33.2 % [10]. Lee et al. [11] fabricated platinum nanoparticle/self-doping PANi composite-based counter electrodes for dye-sensitized solar cells. Xiao et al. synthesized high performance dual function of PANi by using a two-step cyclic voltammetry approach on the fluorinated tin oxide glass substrate. Perovskite sensitized solar cell based PANi delivers photovoltaic conversion efficiency of the order of 7.34 % with long term stability [12].

Motivating from above discussion, we planned to investigate the photovoltaic performance of GO loaded PANi matrix. The main objective of present work is to analyze the effect of addition of GO in PANi matrix in the context of photovoltaic application.

2 Experimental

2.1 Materials preparation

The AR-grade (SD fine India) chemicals were directly procured to use in the present work. The oxidative polymerization method was used to prepare PANi. The aniline monomer and ammonium per sulphate were used with molar ratio 1:1 M for preparation of PANi. The composites between GO and PANi was prepared by ex situ approach. The different composites were prepared by altering the wt% of GO in PANi matrix, with an interval 0.5 wt%. Both these chemicals were mixed in the presence of organic media that is acetone.

2.2 Materials characterization and device fabrication

The X-ray diffraction (XRD) patterns of as-prepared composites were recorded on X-ray diffractometer (Philips PW 1830) using CuK_α radiation ($\lambda = 1.54$ Å). The morphology of samples was analyzed by using field emission-scanning electron microscope (JEOL JSM-7500F). The ultraviolet–visible spectrums of samples were collected from Agilent Cary 60 UV–VIS spectrophotometer. Similarly, Raman spectra of samples were acquired from Bruker Raman spectrometer of wavelength 523 nm. Thermo gravimetric-differential thermal analysis was performed on a Shimadzu DTG-60h thermal analyzer under nitrogen atmosphere. The photovoltaic response of samples tested in dark condition. The various photocell parameter such as short circuit current (I_{SC}), open circuit voltage (V_{OC}), fill factor (FF), and power conversion efficiency (η) were estimated from IV curve. The doctor blade technique was adopted to fabricate photovoltaic cell with architecture ITO/GO–polyaniline/Aluminum.

3 Results and discussion

Figure 1 depicts the XRD patterns of PANi, different samples of GO loaded to PANi matrix and pristine GO. The peak position and relative intensity of characteristics peaks of graphene oxide at 26.2° and 45.3° reflects structural purity of graphene oxide. No other impurity peak is present in XRD pattern of graphene oxide. Similarly, XRD

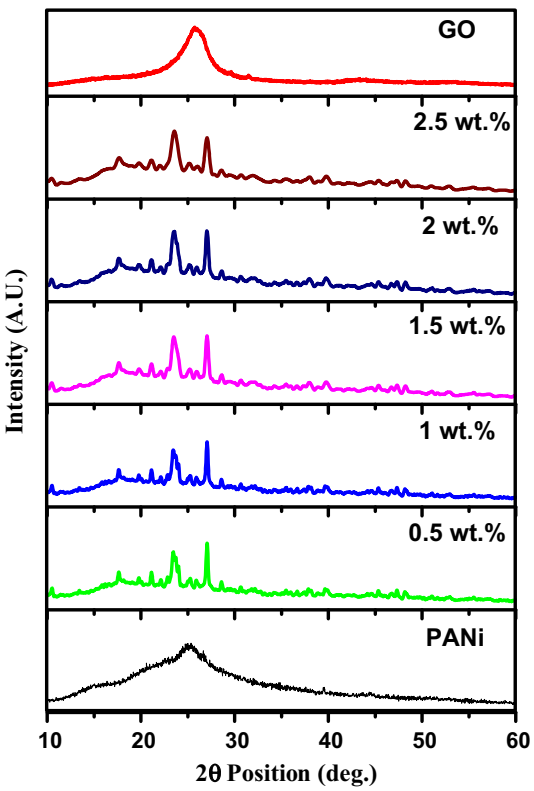

Fig. 1 XRD patterns of PANi, different samples of wt% of GO loaded PANi matrix and GO

pattern of PANi shows amorphous nature and comprises broad hump between 2θ-range 20°–30°. After addition of GO in PANi matrix, some sharp peaks appears on the broad hump of PANi, which directly reflects that degree of crystallinity improves with the addition of GO. As polymeric systems are neither fully crystalline nor fully amorphous, thus the crystallinity is expressed in terms of a degree of crystallinity that quantifies the extent up to which material is crystalline. The improvement in crystallinity is responsible for rough surface. The main change in XRD pattern of GO loaded PANi matrix is that peak width changes with GO concentration. The minute observation of XRD patterns of all five composites shows that peak width of increase with wt% of GO in PANi matrix, reflects that GO nicely incorporated in PANi matrix.

Figure 2a–e represents FE-SEM micrographs of different wt% of GO from 0.5 to 2.5 wt% of interval 0.5 wt% incorporated PANi matrix. All SEM micrograph (Fig. 2a–e) clearly shows that petals or sheets formation of resultant product. Similarly, SEM images (Fig. 2a–e) represent that irregularness in shape and size observed in all samples. Similarly, the surface morphology of product is rough, which is supported by XRD analysis. Such type of morphology is preferred for PV application due to graphene based composites can significantly expand the absorption spectrum of electromagnetic radiation. It is well known phenomenon that graphene in composite state interacts overall weakly via van der Waals interaction. According to Density Functional Theory, no charge transfer is possible until charge redistribution happen within graphene layer. Addition of impurity in pristine graphene system results in the well-defined electron–hole puddles. Therefore, optical characteristics of GO loaded PANi matrix improved for photovoltaic application [13].

Raman spectroscopy is effective tool to analyze carboneous materials. Figure 3a–e shows Raman spectra of GO loaded PANi matrix, which comprises vibration modes of PANi emeradine and characteristics band of GO sheets. In Fig. 3a–e, band appears around 1590 cm^{-1} is results from C–N stretching vibration from benzenoid. In addition to this band, D-band appears at 1325 cm^2 and G band at 1597 cm^2 in Raman spectrum of all samples, as shown in Fig. 3a–e. These bands are characteristics signature of GO. The D band shows that conversion of a sp^2-hybridized carbon to a sp^3-hybridized carbon [14]. Moreover, G band shows that in-plane bond-stretching motion of the pairs of

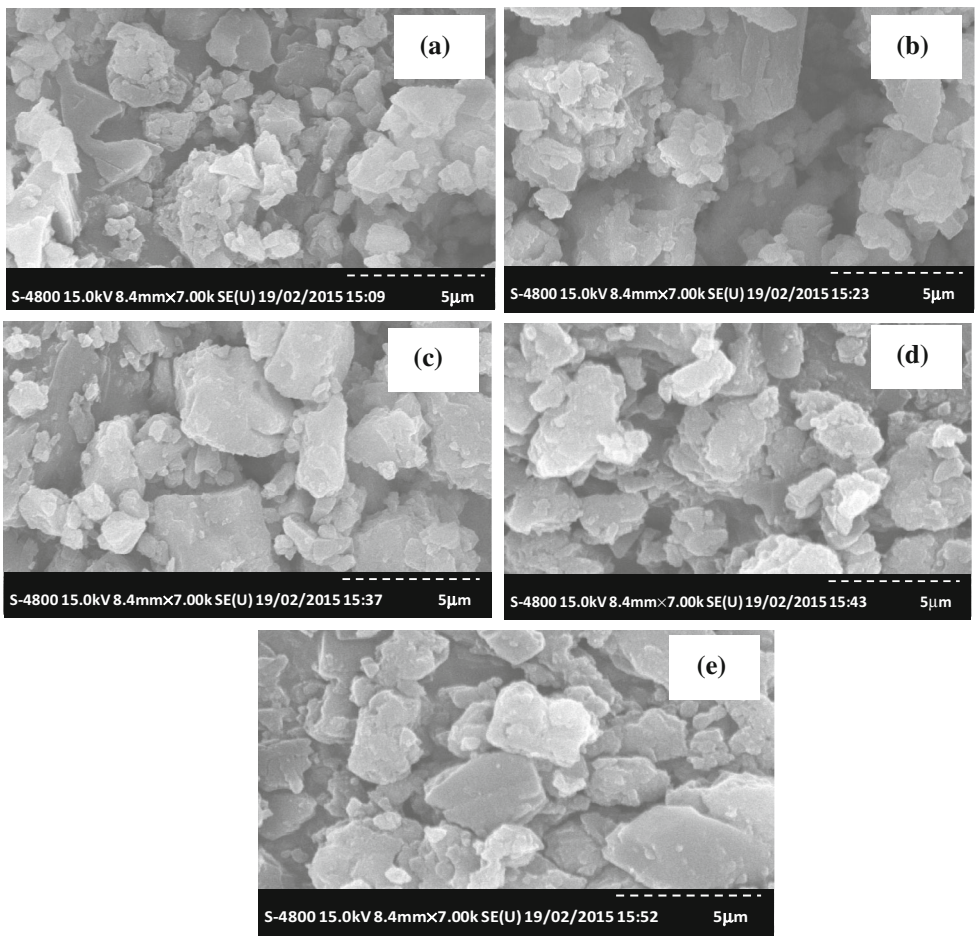

Fig. 2 FE-SEM images of different wt% of **a** 0.5 wt%, **b** 1 wt%, **c** 1.5 wt%, **d** 2 wt% and **e** 2.5 wt% of GO loaded PANi matrix

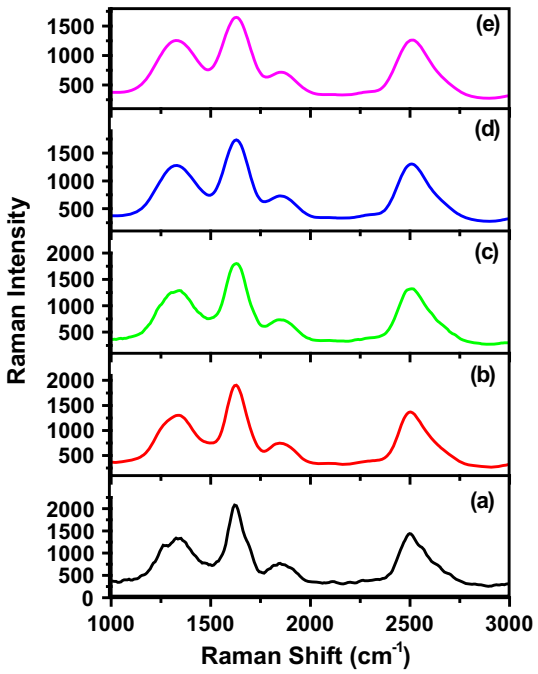

Fig. 3 Raman spectrum of different wt% of GO loaded PANi matrix

C sp^2 atoms, which results from E_{2g} phonons. The width of resultant characteristics peaks increases with GO concentration, which shows that density of E_{2g} phonons increases [15].

Figure 4 shows the TG–DTA pattern of 2.5 wt% GO loaded PANi matrix, which is optimized in power conversion efficiency, which is discussed later. The sample shows 6.79 % of mass loss up to 460 K. The mass loss up to 373 K, is assigned to removal water molecules from GO loaded PANi matrix. The endothermic peak on DTA curve at 361 K, is related with elimination of constituted water molecules from GO loaded PANi matrix. The mass loss again observed beyond 475 K, which is continuing up to 675 K. The endothermic peak at 561 K, is ascribed to the glass transition temperature [16].

Figure 5a–e shows that UV–VIS spectrum of different wt% of GO from 0.5 to 2.5 wt% by interval of 0.5 wt% loaded PANi matrix recorded in the range 190–650 nm. It is observed that absorption coefficient magnitude nearly linear in the range 400–600 nm, and it starts to increase again. The absorption curve of samples shows broad peaks in the range 200–225 nm, which attributed to π–π* transition in polymeric materials [17].The absorption higher for the sample with smallest percentage of GO is observed in Fig. 5a–e. This suggest that GO is less coupled with PANi matrix. Thus, the absorption for 0.5 wt% of GO loaded PANi matrix is high and it decreases with addition of GO in PANi matrix [18].

The magnitude of power conversion efficiency is function of electron transfer between GO and PANi. The valence band edge of PANi is lower in energy than that of GO, but as graphene is two dimensional materials, the gap separation is small. Therefore, the charge separation is increased, which also reduces radiative recombination. In our present work, all this information extracted from PL spectra. PL spectra of GO loaded PANi matrix at different wt% concentration are presented in Fig. 6a–e. The PL spectra of composites samples show a prominent and broad peak at 410 nm in Fig. 6a–e. The critical observation of spectra shows that PL intensity increases with wt% of GO in PANi matrix. This increase in intensity assigned to increase in rate of electron–hole pair separation. Therefore, addition of GO in PANi matrix, results in desirable for enhancement of power conversion efficiency.

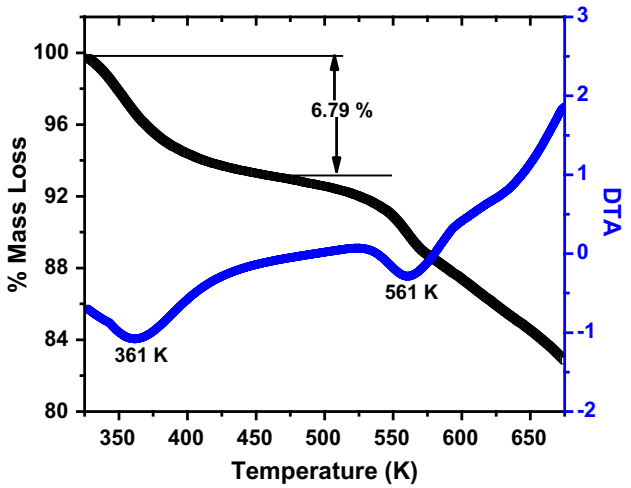

Fig. 4 TG–DTA of 2.5 wt% of GO loaded PANi matrix

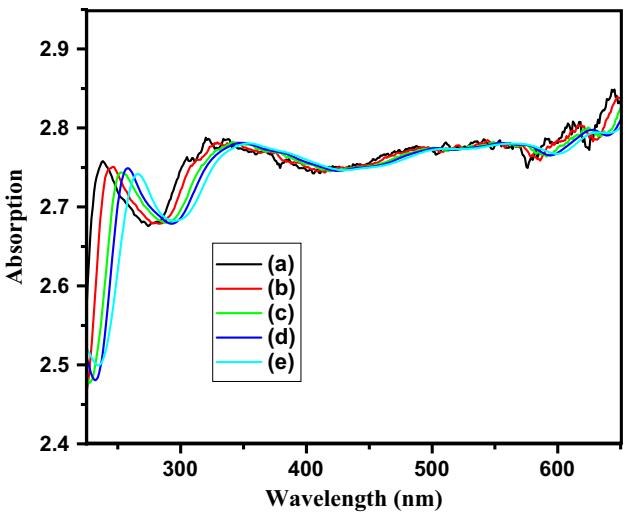

Fig. 5 UV–VIS spectrum of different wt% of GO loaded PANi matrix

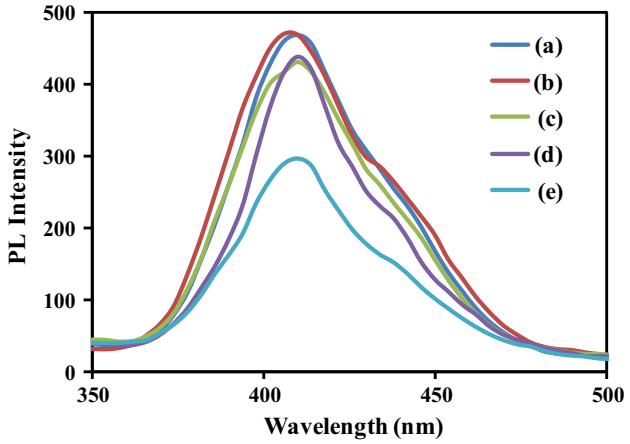

Fig. 6 PL spectra of GO loaded PANi matrix with different concentrations of GO

Current–voltage (I–V) curves of the GO loaded PANi matrix based photovoltaic cells at room temperature (298 K) are shown in Fig. 7. I–V response of fabricated PV cell was done using incandescent light bulb radiating light power of 0.0204 W/m^2, measured using the LUX meter. The bulb and photovoltaic cell separation was 30 cm. The various PV properties of PV diodes such as open circuit voltage (V_{OC}), short circuit current (I_{SC}), fill factor (FF), and power conversion efficiency (η) measured under above discussed conditions. The response of PV cell tested for several times, but no significant deviation in result observed. The fill factor determined using relation Eq. (1) [19]:

$$FF = \frac{I_{MAX} \times V_{MAX}}{I_{SC} \times V_{OC}} \tag{1}$$

The power conversion efficiency (η) calculated using the relation Eq. (2) [20],

$$\%\eta = \left(\frac{I_{SC} \times V_{OC} \times FF}{P_{in}}\right) \times 100 \tag{2}$$

The maximum value of short-circuit current (I_{SC}) was found to be 110.8 μA for 1.5 wt% concentration of GO in PANi matrix. Similarly, the maximum value of $V_{OC} = 214.9$ mV is associated with 2 wt% GO loaded PANi matrix.

Table 1, shows that %η of PV cell increase smoothly with increasing concentration of GO wt% in PANi matrix (Fig. 8). The 2.5 wt% GO loaded PANi matrix produce %η of the order of 0.0452, which may attributed to efficient absorption characteristics of matrix in visible region light. It is also observed that absorption characteristics of matrix increase with increasing wt% GO in PANi matrix. The irregularity is variation of Isc and Voc is attributed to change thickness of sandwiched material between electrodes. Similar finding are reported by Zhao et al. [21] for PANi-based buffer layer system.

The lower value of power conversion efficiency is attributed to the inefficient hole collection by GO from PANi. Another possible reason for the lower efficiency is energy gaps difference in between the GO and PANi, which responsible for poor cell performance. The solution for this issue is that to regulate the thickness of sandwiching layer. Because thickness has direct relation with the hole conduction and density [22]. The efficiency of the fabricated graphene oxide–polyaniline based PV cell is quite low, but it is noteworthy to point two things that used materials system is nontoxic and easy to tune band gap in the visible and infrared regions. By improving the light absorption properties of graphene oxide–polyaniline, we expect significant enhancement in power conversion efficiency [23].The similar conclusion was made by Dutta et al. [24] reported that low power conversion efficiency results from inefficient hole collection in materials.

The %IPCE is measurement is mainly based on three process, migration/diffusion of the photogenerated excitations, exciton uncoupling and charge separation and collection of charges at ITO and Al electrodes also known as charge-trapping sites or 'dead ends'. Figure 9 shows the incident photon power conversion efficiency (%IPCE) spectra of different wt% of GO loaded PANi matrix. The %IPCE is calculated using the relation Eq. (3) [25],

$$\%IPCE = \frac{I_{SC}}{P_{in}} \times \frac{1240}{\lambda\,(\text{nm})} \times 100 \tag{3}$$

where, I_{SC} is short circuit current, P_{in} is power incident and λ is wavelength. The %IPCE values decreases gradually as a function of wavelength. The value of %IPCE initially very large for lower side wavelength and it is decreases for longer wavelength. The decreasing %IPCE with wavelength is ascribed to inefficient charge transport properties in the composite. The magnitude of %IPCE is highest for 2.5 wt% GO loaded PANi matrix.

The variation in indirect band gap GO loaded PANi matrix is checked over energy range 1.75–6 eV by plotting square root of the IPCE versus photon energy. This curve is nearly linear up to 6 eV. Both these parameters shows that selected materials for present work that is GO–PANi composites exhibits good optical activity for PV application. The linear increase in value of SQRT(%IPCE) indicates indirect transitions also present in sample.

Figure 10 depicts the optical conductivity curves for different wt% of GO from 0.5 to 2.5 wt% by interval of 0.5 wt% loaded PANi matrix. The optical conductivity is estimated using the following relation Eq. (4) [26],

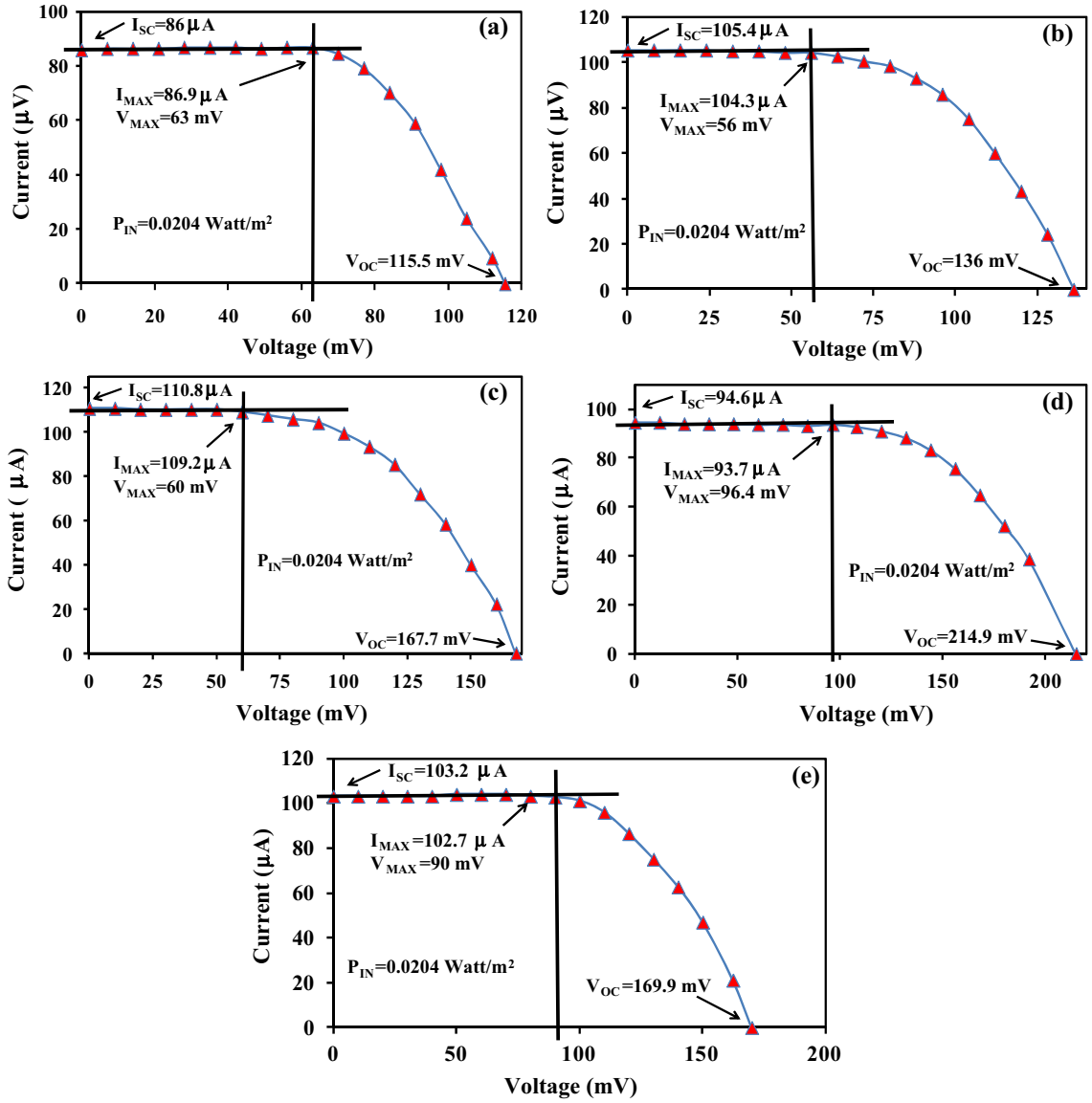

Fig. 7 Photovoltaic response of different wt% of GO loaded PANi matrix sandwiched in architecture ITO/GO–PANi/aluminum

Table 1 Values of I_{sc}, V_{oc}, I_{max}, V_{max}, %FF and %η of photovoltaic cell with architecture ITO/GO–polyaniline/aluminum

Sample (wt%)	I_{sc} (μA)	V_{oc} (mV)	I_{max} (μA)	V_{max} (mV)	FF	%η
0.5	86	115.6	86.9	63	0.551	0.0268
1	105.4	136	104.3	56	0.407	0.0285
1.5	86	115.6	86.9	63	0.552	0.0321
2	94.6	214.9	93.7	96.4	0.444	0.044
2.5	103.2	169.9	102.7	90	0.527	0.0452

$$\sigma = \frac{\alpha c n}{4\pi} \tag{4}$$

where α is % transmission, c is velocity of light and n is refractive index. The value of refractive index computed using the relation Eq. (5),

$$n = \frac{1}{\%T} + \sqrt{\frac{1}{\%T} - 1} \tag{5}$$

where %T is transmission through different matrix.

The optical conductivity values increases smoothly in the range 190–225 nm for all samples (0.5–2.5 wt%).

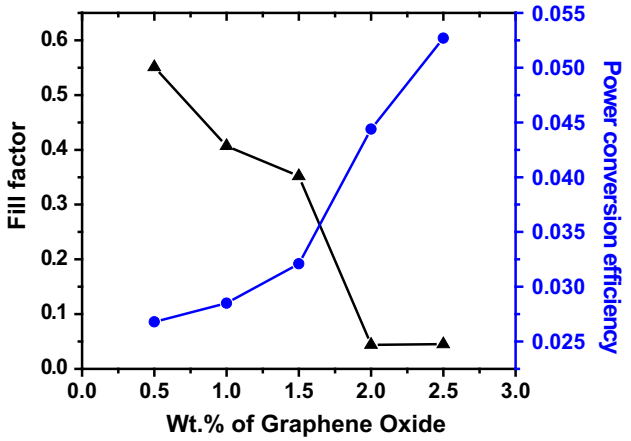

Fig. 8 Variation of fill factor and power conversion efficiency with wt% of GO in PANi matrix

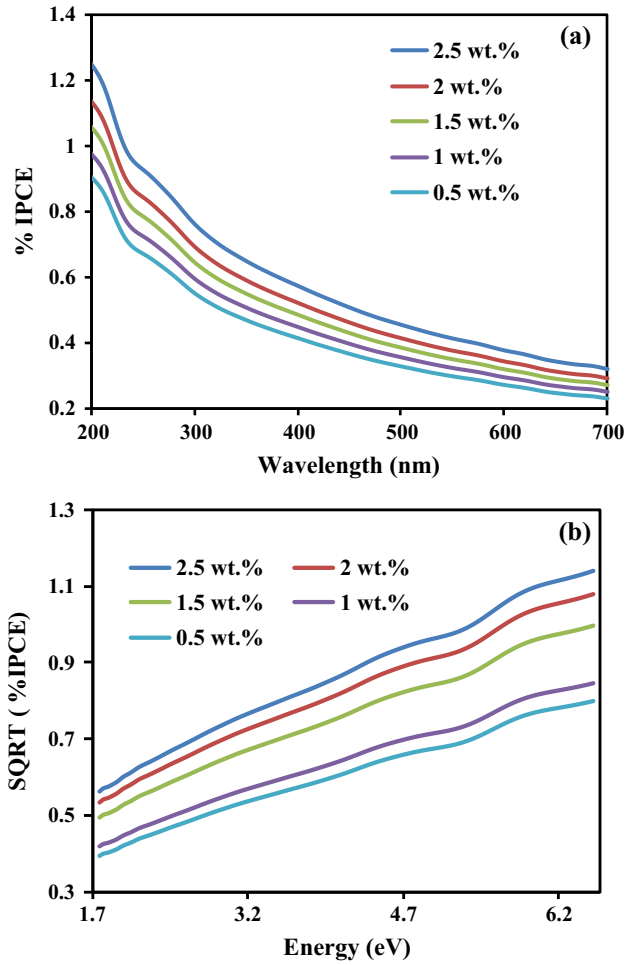

Fig. 9 **a** Variation of %IPCE with wavelength of different wt% of GO loaded PANi matrix based PV cell and **b** variation of SQRT (IPCE) with energy

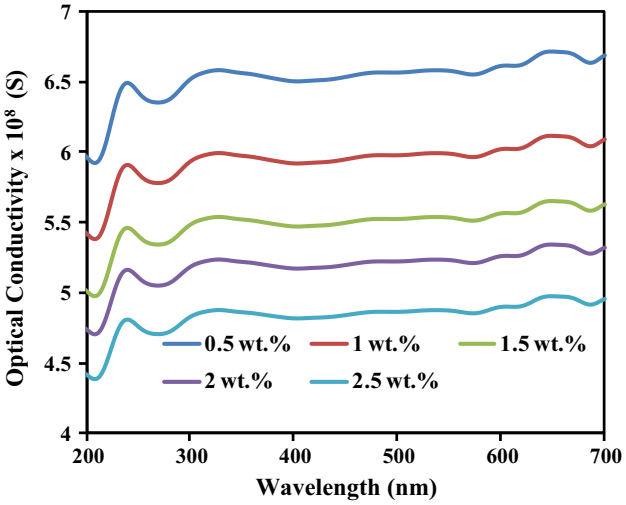

Fig. 10 Variation of optical conductivity with wavelength for different wt% of GO loaded PANi matrix based PV cell

Similarly, the optical conductivity curves of all samples have nearly flat nature in visible region 400–600 nm, which reflects that free charge carriers are continuously generated for longer wavelength. This is helpful for PV application. The highest optical conductivity was obtained for 0.5 wt% of GO loaded PANi matrix.

4 Conclusions

In the present work, we successfully engineered PV cells based on architecture ITO/GO–polyaniline/Al. The power conversation efficiency and fill factor value shows good dependence on concentration of GO in PANi matrix. The power conversation efficiency value ranges between 0.0268 and 0.0452 under light illumination (0.0204 W/m^2). The concentration of GO in PANi matrix significantly affects the photovoltaic performance of fabricated cells. The present work has implications for cost effective and efficient next generation photovoltaic cell.

Acknowledgments The authors appreciate help of Sophisticated Test and Instrumentation Centre and Visvesvaraya National Institute of Technology, Nagpur for providing necessary characterizations for present research work. One of the authors Dr. S.P. Yawale is thankful to University Grants Commission (UGC), New Delhi for providing major research project.

References

1. S. Ebrahim, M. Soliman, M. Anas, M. Hafez, T.M. Abdel-Fattah, Int. J. Photoenergy **2013**, 906820 (2013)

2. S. Mozaffari, M.R. Nateghi, M. Borhanizarandi, Recent Adv. Environ. Sci. Biomed. **41**, 121 (2010)
3. T.M. Abdel-Fattah, S. Ebrahim, M. Soliman, M. Hafez, ECS J. Solid State Sci. Technol. **2**, 13 (2013)
4. O. Abdulrazzaq, S.E. Bourdo, V. Saini, V.G. Bairi, E. Dervishi, T. Viswanathan, Z.A. Nima, A.S. Biris, Energy Technol. **1**, 463 (2013)
5. K. Huang, C. Hu, C. Tseng, C. Liu, M. Yeh, H. Wei, C. Wang, R. Vittal, C. Chucd, K. Ho, J. Mater. Chem. **22**, 14727 (2012)
6. S. Mangal, S. Adhikari, P. Banerji, Appl. Phys. Lett. **94**, 223509 (2009)
7. F. Huang, Q. Li, G.J. Thorogood, Y. Cheng, R.A. Caruso, J. Mater. Chem. **22**, 17128 (2012)
8. J. Wu, Y. Li, Q. Tang, G. Yue, J. Lin, M. Huang, L. Meng, Sci. Rep. **4**, 4028 (2014)
9. K. Inoue, T. Akiyama, A. Suzuki, T. Oku, Jpn. J. Appl. Phys. **51**, 1 (2012)
10. R.A. Elgani, M.H.M. Hilo, A.A. Hassan, M.D.A. Allah, Nat. Sci. **5**, 52 (2013)
11. R. Lee, C. Chi, Y. Hsu, J. Nanopart. Res. **15**, 1733 (2013)
12. Y. Xiao, G. Han, Y. Chang, H. Zhou, M. Li, Y. Li, J. Power Sources **267**, 1 (2014)
13. W. Hu, Z. Li, J. Yang, J. Chem. Phys. **138**, 124706 (2013)
14. A. Ferrari, J. Robertson, Phys. Rev. B **61**, 14095 (2000)
15. L. Cancado, M. Pimenta, B. Neves, M. Dantas, A. Jorio, Phys. Rev. Lett. **93**, 247401 (2004)
16. Y.N. Qi, F. Xu, H.J. Ma, L.X. Sun, J. Zhang, T. Jiang, J. Therm. Anal. Calorim. **91**, 219 (2007)
17. A. Kaushik, J. Kumar, M.K. Tiwari, R. Khan, B.D. Malhotra, V. Gupta, S.P. Singh, J. Nanosci. Nanotechnol. **8**, 1757 (2008)
18. J. Du, X. Lai, N. Yang, J. Zhai, D. Kisailus, F. Su, D. Wang, L. Jiang, ACS Nano **5**, 590 (2011)
19. T. Salmi, M. Bouzguenda, A. Gastli, A. Masmoudi, Int. J. Renew. Energy Res. **2**, 213 (2012)
20. M. Seifi, A. Soh, N. Izzrib, A. Wahab, M.K.B. Hassan, Int. J. Electr. Robot. Electron. Commun. Eng. **7**, 97 (2013)
21. W. Zhao, L. Ye, S. Zhang, B. Fan, M. Sun, J. Hou, Sci. Rep. **4**, 6570 (2014)
22. C.J. Brabec, A. Cravino, D. Meissner, N.S. Sariciftci, T. Fromherz, M.T. Rispens, L. Sanchez, J.C. Hummelen, Adv. Funct. Mater. **11**, 374 (2001)
23. X. Yan, X. Cui, B.S. Li, L.S. Li, Nano Lett. **10**, 1869 (2010)
24. M. Dutta, S. Sarkar, T. Ghosh, D. Basak, J. Phys. Chem. C **116**, 20127 (2012)
25. Q.W. Tang, H.Y. Cai, S.S. Yuan, X. Wang, J. Mater. Chem. A **1**, 317 (2013)
26. N.A. Bakr, A.M. Funde, V.S. Waman, M.M. Kamble, R.R. Hawaldar, D.P. Amalnerkar, S.W. Gosavi, S.R. Jadkar, Pramana **76**, 519 (2011)